

Dynamics of a vortex filament in a shear flow

By HASSAN AREF AND EDWARD P. FLINCHEM

Division of Engineering, Brown University, Providence, R.I. 02912

(Received 16 December 1983)

Motions of a single vortex filament in a background flow are studied by numerical simulation of a set of model equations. The model, which in essence is due to Hama, treats the self-interaction of the filament through the so-called ‘localized-induction approximation’ (LIA). Interaction with the prescribed background field is treated by simply advecting the filament appropriately. We are particularly interested in elucidating the evolution of sinuous vortices such as the ‘wiggle’ seen by Breidenthal in the transition to three-dimensionality in the mixing layer. The model studied embodies two of the simplest ingredients that must enter into any dynamical explanation: induction and advection. For finite-amplitude phenomena we make contact with the theory of solitons on strong vortices developed by Betchov and Hasimoto. In a shear, solitons cannot exist, but solitary waves can, and their interactions with the shear are found to be key ingredients for an understanding of the behaviour of the vortex filament. When sheared, a soliton seems to act as a ‘nucleation site’ for the generation of a family of waves. Computed sequences are shown that display a remarkable morphological similarity to flow-visualization studies. The present application of fully nonlinear dynamics to a model presents an attractive alternative to the extrapolations from linearized stability theory applied to the full equations that have so far constituted the theoretical basis for understanding the experimental results.

1. Introduction

In a series of papers written in the early 1960s Hama and collaborators investigated the deformation of a single, strong vortex filament idealized as a space curve using a certain asymptotic theory for the self-induced motion of the vortex now commonly referred to as the ‘localized-induction approximation’† (see e.g. Hama 1963; Arms & Hama 1965). LIA captures the leading-order behaviour of the Biot–Savart induction law, which is believed to govern the large-scale bending and flexing of a concentrated vortex. Several years later Hasimoto (1972) showed that the LIA equations, when written in terms of the local geometric quantities curvature and torsion as first suggested by Betchov (1965), are equivalent under a certain transformation to the cubic Schrödinger equation in one space dimension. It follows from this observation and the work of Zakharov & Shabat (1972) that any perturbation of a concentrated vortex filament should evolve into one or more solitons, which for this case are localized helical twists of the vortex core. This important prediction seems to have been largely ignored for a decade following Hasimoto’s (1972) work.

Recent experiments (Hopfinger & Browand 1982; Hopfinger, Browand & Gagne

† Henceforth abbreviated to LIA.

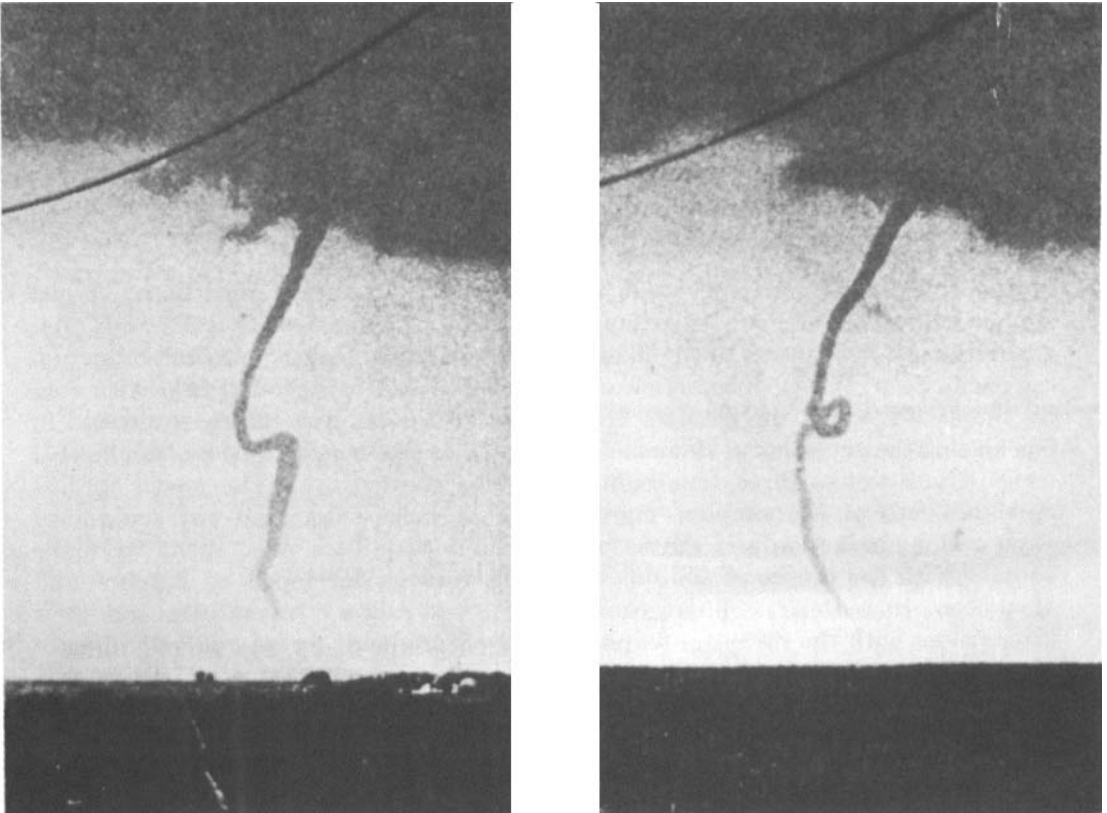


FIGURE 1. Two photographs of a tornado near Braman, Oklahoma (11 May 1978) showing a distinct large-amplitude localized twist of the vortex core. Photographs by T. Goggin, *Newkirk Herald Journal* (reproduced with permission).

1982; Maxworthy, Hopfinger & Redekopp 1985) have provided considerable evidence that helical-twist solitons or closely related solitary waves do indeed occur on concentrated vortices in ordinary fluids, although coupling to the degrees of freedom of the vortex core frequently complicates the simple idealized picture presented by LIA theory. Rotating superfluid helium seems a prime candidate for application of these ideas, since the vortices have cross-sections of atomic dimensions (cf. Donnelly 1967), but such vortices are difficult to visualize and the existence of solitary twists must be inferred by indirect means. Concentrated vortices in ordinary fluids, e.g. the vortices shed from the body and wings of aircraft or from the hulls of ships and from various types of propellers, frequently appear to support one or more standing or propagating twist waves. Pictures and ciné films of tornadoes and waterspouts in the decaying stage, when the vortex is thin and ropelike, commonly reveal systems of transverse waves propagating up or down (see e.g. figures 13 and 14 of Golden & Purcell (1978) or figure 4 of Peterson *et al.* (1979)). The clearest instance of a localized twist on a tornado that we have seen is reproduced as figure 1. These are pictures of the tornado at Braman, Oklahoma (11 May 1978) taken by T. Goggin of the *Newkirk Herald Journal* (and published previously by Wilson, Pearson & Ostby 1979). We suggest that the disturbance seen here is an example of a wave very closely related to the Hasimoto soliton.

The phenomenology just described has inspired experimental and theoretical

investigations aimed at understanding the modifications to LIA predictions that must arise from effects associated with finite vortex cores, fluid viscosity, axial flow etc. (Maxworthy *et al.* 1985; Leibovich & Ma 1983). The tentative conclusion of these investigations is that solitary waves do exist on concentrated vortices in ordinary fluids, but that at small amplitudes they are modified relative to the LIA predictions by the finite core.

The present paper is a report on some simple numerical experiments that we have been conducting in an attempt to relate the elegant theory of Betchov (1965) and Hasimoto (1972) and in particular the concept of solitons on vortices to certain aspects of the phenomenology seen in laboratory shear flows. We have returned to a model, introduced already by Hama (1963), in which the vortex filament moving itself through LIA is also subjected to a background shear flow. For this model we can show through numerical calculations of the initial-value problem that solitons will act as ‘nucleation sites’ for a system of transverse, dispersive waves along the vortex. When a shear-layer ‘background’ is used the resulting deformation of the vortex bears a striking resemblance to detailed flow-visualization studies by Breidenthal (1978, 1979) of the onset of three-dimensional instability on a two-dimensional vortex ‘roller’ in a mixing layer. In effect what we have documented is a mechanism through which localized twists (or similar perturbations) on an essentially two-dimensional vortex can develop into an extended transverse wave on the vortex. This mechanism should be observable in many flow situations, of which the mixing layer is the most readily available. Our results on a vortex filament in a background shear flow appear in §2.4.

We emphasize that these results pertain to a particular model. And, while we have no doubts that they are correct for the model, there remains the important and non-trivial issue of how the model relates to the full three-dimensional Euler equation. One problem is that the background or mean flow that is relevant in a shear layer also has vorticity, whereas the only evolving vorticity in the model is associated with the concentrated filament. This question is taken up in §2.1, where, after a brief review of LIA, we present some simple order-of-magnitude estimates suggesting that the terms retained in Hama’s (1963) model describe a possible balance in the full dynamics.

We describe the numerical discretization procedure employed in §2.2, and in §2.3 we show several simulations of two-soliton collisions on an unsheared filament. Although such collision processes are in principle just transcriptions of solutions to the cubic Schrödinger equation, they are of interest both from the standpoint of recent laboratory experiments and from the standpoint of the formal mathematical theory of the cubic Schrödinger equation. Summary, conclusions and possible extensions of the work reported are collected in §3.

2. Numerical experiments on vortex-filament motion

In this section we describe the theoretical ideas behind our model for vortex-filament motion, its numerical implementation and the main results that we have obtained so far.

2.1. Localized-induction approximation

It is well known that, if a vortex filament is idealized as a space curve, the Biot–Savart integral which gives the velocity field surrounding it diverges if the ‘field point’ at which the velocity is desired coincides with a ‘source point’ on the filament. Hence,

to deduce the motion of the filament under its self-induced velocity, an asymptotic analysis, in which the space curve is replaced by a family of ever thinner tubes, is required.

It is also well known (Arms & Hama 1965; Betchov 1965; Batchelor 1967) that the leading term to emerge from such an analysis is a local term, and that by using Helmholtz' theorem for the motion of the vortex one obtains the following velocity law,

$$\frac{\partial \mathbf{x}}{\partial t} = C\Gamma\kappa\mathbf{b}, \quad (1)$$

for each point \mathbf{x} on the filament. Here Γ is the circulation of the vortex, κ is the local curvature and \mathbf{b} is the local unit binormal. The non-dimensional constant C is the asymptotic expansion parameter (essentially the logarithm of the ratio of filament radius of curvature to tube cross-sectional radius), and is thus 'large' but of unknown magnitude. For a single filament the actual value of C does not matter for most purposes, since C can be absorbed into a rescaling of the time variable, i.e. we set

$$\theta = C\Gamma t \quad (2)$$

(where θ has the physical dimensions of area), and then

$$\frac{\partial \mathbf{x}}{\partial \theta} = \kappa\mathbf{b}. \quad (3)$$

Note that, since the velocity vector for points on the vortex filament is always perpendicular to the filament, a vortex evolving under LIA does not stretch itself.

It is clear that the approximations implied by (1) or (3) ignore several aspects of the dynamics of real concentrated vortices. Most obviously, the deformation of the vortex core is not represented. This problem has received considerable attention, particularly in purely two-dimensional flows (for reviews see e.g. Zabusky 1981; Aref 1983). Viscous diffusion and the possible effects of axial flow are also ignored. Moreover, the approximation is given by a local term and thus will not be valid when two distant portions of the filament approach each other closely. In spite of all these shortcomings (which were already realized in the 1960s), LIA solutions seem to provide useful clues to the large-scale bending and flexing of a concentrated vortex. There are indeed several examples of simple solutions to the LIA which are known to have close counterparts in the full theory of vortex tubes evolving under the three-dimensional Euler equation. These examples include the circular vortex ring, the elliptical vortex ring (Dhanak & Bernardinis 1981) and the helical vortex (Hardin 1982). For a comprehensive study of steady-state vortex-filament configurations and their stability within the framework of LIA see the papers by Kida (1981, 1982).

As first shown by Betchov (1965), it is illuminating to combine (3) with the Frenet-Serret formulae of differential geometry (Eisenhart 1960). After a straightforward calculation we then obtain the following coupled system of partial differential equations for the filament curvature κ and torsion τ :

$$\dot{\kappa} + (\kappa\tau)' = -\kappa'\tau, \quad \dot{\tau} - \left(\frac{\kappa''}{\kappa} - \tau^2 + \frac{1}{2}\kappa^2\right)' = 0. \quad (4a, b)$$

Here a dot denotes a partial derivative with respect to θ , (2), and a prime a derivative with respect to arclength along the curve. Equations (4) are usually referred to as *Betchov's intrinsic equations*.

Historically some seven years passed between Betchov's (1965) derivation of (4) and the realization by Hasimoto (1972) that, if one defined a 'wave function'

$$\psi(s, \theta) = \kappa(s, \theta) \exp \left\{ i \int^s \tau(s', \theta) ds' \right\}, \quad (5)$$

where κ, τ evolve according to (4), then

$$\frac{1}{i} \frac{\partial \psi}{\partial \theta} = \frac{\partial^2 \psi}{\partial s^2} + \frac{1}{2} |\psi|^2 \psi. \quad (6)$$

Recently Spiegel (1980) has discussed in general terms the existence of a 'Madelung transformation' such as (5) connecting a wave equation of Schrödinger type (6) to a set of evolution equations of the form (4). Lamb (1977) has considered other generalizations of the connection between a wave equation and motions of a space curve exemplified by Hasimoto's (1972) transformation.

The reduction of (4) to (6) in spite of its formal elegance is not terribly useful for numerical calculations since it is in general cumbersome and inefficient to reconstruct the space curve at every time step from the values of κ and τ obtained through solving (6) for ψ . However, since (6) is integrable (Zakharov & Shabat 1972), this reduction does show that vortex filaments moving according to LIA support solitons (which a more detailed investigation reveals are localized helical twists with a speed of propagation proportional to the torsion). This property is useful in testing a code constructed on the basis of (1), as we shall see in §2.3.

As discussed in §1, we are particularly interested in a modification of (1) to a model suitable for following the evolution of a vortex filament embedded in a shear flow. Thus, following Hama (1963), we shall consider the equation of motion

$$\frac{\partial \mathbf{x}}{\partial t} = C\Gamma\kappa\mathbf{b} + \mathbf{U}_{\text{ext}}(\mathbf{x}), \quad (7)$$

where \mathbf{U}_{ext} is a prescribed flow. In general \mathbf{U}_{ext} will lead to stretching of the filament. In our applications in §2.4 we shall set

$$\mathbf{U}_{\text{ext}}(x, y, z) = U_0 \tanh\left(\frac{y}{\Delta}\right) \hat{\mathbf{i}}, \quad (8)$$

where $\hat{\mathbf{i}}$ is a unit vector in the x -direction and U_0, Δ are constant parameters. This flow represents the 'mean' or 'background' flow in a free shear layer.

In order to understand the nature of the approximations implicit in this model it is illuminating to compare it with what one would obtain by formally decomposing the velocity and vorticity in the three-dimensional Euler equation into a sum of two contributions. Thus we consider the vorticity equation

$$\frac{\partial}{\partial t} \boldsymbol{\omega} + \mathbf{u} \cdot \nabla \boldsymbol{\omega} = \boldsymbol{\omega} \cdot \nabla \mathbf{u} \quad (9)$$

and let $\mathbf{u} = \mathbf{u}_1 + \mathbf{u}_2$, $\boldsymbol{\omega} = \boldsymbol{\omega}_1 + \boldsymbol{\omega}_2$, where $\boldsymbol{\omega}_j = \nabla \times \mathbf{u}_j$, $j = 1, 2$. We substitute this into (9) to obtain

$$\begin{aligned} \frac{\partial}{\partial t} \boldsymbol{\omega}_1 + \frac{\partial}{\partial t} \boldsymbol{\omega}_2 + \mathbf{u}_1 \cdot \nabla \boldsymbol{\omega}_1 + \mathbf{u}_2 \cdot \nabla \boldsymbol{\omega}_2 + \mathbf{u}_1 \cdot \nabla \boldsymbol{\omega}_2 + \mathbf{u}_2 \cdot \nabla \boldsymbol{\omega}_1 \\ = \boldsymbol{\omega}_1 \cdot \nabla \mathbf{u}_1 + \boldsymbol{\omega}_2 \cdot \nabla \mathbf{u}_2 + \boldsymbol{\omega}_1 \cdot \nabla \mathbf{u}_2 + \boldsymbol{\omega}_2 \cdot \nabla \mathbf{u}_1. \end{aligned}$$

We now assume that the field subscripted 2, the ‘background’, is itself a (steady) solution of (9). Then the second and fourth terms on the left-hand side cancel the second term on the right, and we are left with

$$\frac{\partial}{\partial t} \boldsymbol{\omega}_1 + \mathbf{u}_1 \cdot \nabla \boldsymbol{\omega}_1 - \boldsymbol{\omega}_1 \cdot \nabla \mathbf{u}_1 + \mathbf{u}_2 \cdot \nabla \boldsymbol{\omega}_1 = \boldsymbol{\omega}_1 \cdot \nabla \mathbf{u}_2 + \boldsymbol{\omega}_2 \cdot \nabla \mathbf{u}_1 - \mathbf{u}_1 \cdot \nabla \boldsymbol{\omega}_2.$$

The model in (7) is designed to treat the terms on the left-hand side of this equation and ignore those on the right. (We show below that this is a reasonable way to proceed by providing order-of-magnitude estimates for all terms.) On the left-hand side the first three terms are modelled by LIA (which, in fact, says that the *stretching* contributed by the term $\boldsymbol{\omega}_1 \cdot \nabla \mathbf{u}_1$ vanishes). The fourth term describes the advection by the background. On the right-hand side the second and third terms describe the action of the vortex-filament velocity field on the background vorticity. These terms are ignored. Finally the term $\boldsymbol{\omega}_1 \cdot \nabla \mathbf{u}_2$, which one might intuitively have assumed would dominate the stretching and reorientation of filament vorticity, is ignored and the background is reduced to the role of an extraneous advecting agent.

In order to provide some legitimacy to the model (7) (other than historical precedent) consider instead of a vortex filament a slender vortex tube of diameter δ (and circulation Γ). Using (8) we may then estimate the neglected terms as follows:

$$|\boldsymbol{\omega}_2 \cdot \nabla \mathbf{u}_1| \sim \frac{U_0 \Gamma}{\Delta \delta^2}, \quad |\mathbf{u}_1 \cdot \nabla \boldsymbol{\omega}_2| \sim \frac{\Gamma U_0}{\delta \Delta^2}, \quad |\boldsymbol{\omega}_1 \cdot \nabla \mathbf{u}_2| \sim \frac{\Gamma U_0}{\delta^2 \Delta}.$$

On the other hand, a similar estimate would give

$$|\mathbf{u}_2 \cdot \nabla \boldsymbol{\omega}_1| \sim \frac{U_0 \Gamma}{\delta^3}$$

for the advection term being retained. According to these estimates, the relative magnitudes of neglected to retained terms are

$$\frac{|\boldsymbol{\omega}_2 \cdot \nabla \mathbf{u}_1|}{|\mathbf{u}_2 \cdot \nabla \boldsymbol{\omega}_1|} \sim \frac{|\boldsymbol{\omega}_1 \cdot \nabla \mathbf{u}_2|}{|\mathbf{u}_2 \cdot \nabla \boldsymbol{\omega}_1|} \sim \frac{\delta}{\Delta} \quad \text{and} \quad \frac{|\mathbf{u}_1 \cdot \nabla \boldsymbol{\omega}_2|}{|\mathbf{u}_2 \cdot \nabla \boldsymbol{\omega}_1|} \sim \left(\frac{\delta}{\Delta}\right)^2,$$

both of which are very small when $\delta \ll \Delta$, i.e. when the diameter of the vortex is negligible compared with the spatial scale of the background flow field. Note that so long as \mathbf{u}_2 can be considered linear in y , i.e. $\mathbf{u}_2 = (U_0 y/\Delta, 0, 0)$ (which is true for most of the calculations reported on in §2.4), we have $\mathbf{u}_1 \cdot \nabla \boldsymbol{\omega}_2 = 0$ identically.

These estimates suggest that (7) is a reasonable model of (9), written in terms of Lagrangian coordinates for the vortex filament, valid, roughly speaking, to order δ/Δ . One must, however, keep in mind that emerging transverse oscillations of the vortex will introduce other lengthscales into the problem, and so the estimates above will not be uniformly valid in time. The notion that a background field of scale Δ acts on a small ‘eddy’ of scale $\delta \ll \Delta$ only by advection is familiar from qualitative arguments used in the ‘cascade dynamics’ of fully turbulent flows.

The calculations reported in §2.4 are predicated on (7) being a valid model (for some finite time) of the large-scale motions of a vortex filament in an essentially permanent environment. It seems clear that experimental situations in which this is true can be constructed. However, there are also various shear flows in which such a model seems applicable. The early stages of a mixing layer, for example, appear suitable (although one might be troubled by the asymptotics $\delta \ll \Delta$). When used for such flows the model in (7) is akin to ‘mean-field’ or ‘effective-medium’ theories so popular in many areas of physical science.

2.2. Algorithm for numerical computations

Let the filament be represented by a string of node points uniformly spaced in arclength, $\mathbf{x}_n = \mathbf{x}(n\Delta s)$, where $n = 0, \pm 1, \dots$ and Δs is the arclength spacing. Using standard centred differences

$$\kappa \mathbf{b} = \frac{\partial \mathbf{x}}{\partial s} \times \frac{\partial^2 \mathbf{x}}{\partial s^2} = (\mathbf{x}_{n-1} \times \mathbf{x}_n + \mathbf{x}_n \times \mathbf{x}_{n+1} + \mathbf{x}_{n+1} \times \mathbf{x}_{n-1}) / (\Delta s)^3$$

with a truncation error $O((\Delta s)^2)$. The resulting numerical approximation to (7), viz

$$\frac{d\mathbf{x}_n}{dt} = C\Gamma(\mathbf{x}_{n-1} \times \mathbf{x}_n + \mathbf{x}_n \times \mathbf{x}_{n+1} + \mathbf{x}_{n+1} \times \mathbf{x}_{n-1}) / (\Delta s)^3 + \mathbf{U}_{\text{ext}}(\mathbf{x}_n) \quad (10)$$

preserves the following two important properties of LIA:

$$\frac{\partial \mathbf{x}}{\partial t} \cdot \frac{\partial \mathbf{x}}{\partial s} = 0, \quad \frac{\partial \mathbf{x}}{\partial t} \cdot \frac{\partial^2 \mathbf{x}}{\partial s^2} = 0$$

(in the absence of an external field \mathbf{U}_{ext}) in the sense that

$$\frac{d\mathbf{x}_n}{dt} \cdot (\mathbf{x}_{n+1} - \mathbf{x}_{n-1}) = 0, \quad \frac{d\mathbf{x}_n}{dt} \cdot (\mathbf{x}_{n+1} - 2\mathbf{x}_n + \mathbf{x}_{n-1}) = 0.$$

In the computations reported on below we have used (10) with $C\Gamma = 1$. Periodic boundary conditions are imposed in the z -direction such that with N node points $x_{N+1} = x_1$, $y_{N+1} = y_1$, $z_{N+1} = z_1 + L$, where L is our spanwise spatial window. Time-stepping was performed using the predictor-corrector routine STEP due to Shampine & Gordon (1975). This routine chooses its own order and stepsize according to the values of given error-control parameters. Typically the time integrations proceeded using a third- or fourth-order algorithm. The results shown here were all generated using the CRAY-1 computer at the National Center for Atmospheric Research (NCAR). Preliminary runs were performed on a VAX-11/780 computer using single precision.

When an external velocity field is imposed, the filament stretches, Δs increases, and the node points cease to be uniformly spaced. In order to retain a uniform magnitude of the truncation error along the filament, it was therefore necessary to develop a redistributing subroutine that would place new node points uniformly on the deformed space curve. This was done in a straightforward way using the package CURV from the software collection NSSL distributed by the Scientific Computing Division at NCAR. CURV contains routines to perform cubic-spline fits under tension to a given set of data points. As the calculation progressed we would monitor the distances between adjacent node points and, in particular, the average and root-mean-square deviation of these quantities. When the r.m.s. deviation exceeded a certain small percentage of the mean (usually 1%), redistributing would be invoked and time-stepping reinitiated. This happened readily and repeatedly when a shear was acting on the filament; but never occurred when running 'free' filaments under pure LIA, in accord with the fact that LIA does not lead to vortex stretching. Since, owing to the local interactions, the computational effort per time step of the model considered is proportional to N , the total number of node points, it was found in the present investigation to be expedient to run with a large number of node points (typically 80–300) instead of having schemes for node insertion during a run.

Several detailed quantitative tests were performed to assess how many node points

are necessary to resolve a curved filament adequately. For example, if we consider a vortex ring of radius R , LIA gives a 'theoretical' velocity of translation $V_{\text{th}} = CF/R$. The discretization in the numerical scheme (10), on the other hand, gives a velocity

$$V_{\text{num}} = \frac{CF}{R} \cos \frac{\pi}{N}.$$

This formula, which, of course, agrees with the velocity calculated by our code, shows that using 15 node points one commits a 2% error in the velocity, and using 30 node points the error is less than 1%. Several tests of this type were performed for the standard equilibrium shapes – ring, helix and small-amplitude sine wave (see Batchelor 1967) – and used to provide a rough guide in setting the number of node points for a run (see also §2.3).

2.3. Soliton collisions

As additional checks on the algorithm and code, we computed several sequences showing the collision of two solitons. These runs provide a more comprehensive test, since we are following time-dependent evolution rather than steady-state motion. We have both computed head-on collisions and head-tail collisions where a fast (high-torsion) soliton catches up to, collides with and then leaves behind a slower (low-torsion) soliton. While doing these runs we continually monitored the curvature and torsion of the filament (as a function of arclength). The smoothness of these two quantities gives a very direct impression of the 'quality' of a run. And, indeed, one can produce runs with very similar sequences of space curves but of widely varying 'quality'. In this way monitoring the curvature and torsion has allowed us to 'fine tune' the appropriate settings of important numerical parameters such as the relative accuracy of the time-stepping and the number of node points.

Figure 2 shows plan views (i.e. projections on a (z, x) -plane) of a head-on collision between two opposite but otherwise identical, relatively high-torsion solitons (torsions are ± 10 , with the unit of length taken as the distance L between periodic boundaries). A complicated sequence of events unfolds as the solitons pass through one another. There is a reflection symmetry between the left and right portions of the filament in this run (but the entire filament is being evolved in time). In figure 3 we show corresponding pictures of the filament in a perspective view. The two different views of essentially identical solitons provided by figure 3(a) should be compared to the two views of the twist seen in figure 1. Figure 4 shows stages in the head-on collision of two different solitons in perspective view. Note that the solitons are highly localized entities and that their interaction appears as a short-range effect. Distant portions of the filament and the section of the filament between the solitons remain rectilinear.

In figures 5 and 6 analogous sequences of plan and perspective view, real-space plots are displayed for the head-tail collision of one soliton (of torsion $+2$) with another (of torsion $+10$). This process also is very complex, with the low-torsion soliton winding its way along the filament while the high-torsion soliton comes straight towards it. In both figures 2 (or 3) and 5 (or 6) we have checked in detail the similarity of initial and final states (curvature and torsion) except for phase shifts. These results give us confidence that our code can be used for relatively long-time finite-amplitude simulations.

Soliton collisions have been attempted experimentally by Hopfinger *et al.* (1982) and by Maxworthy *et al.* (1985). In the former paper internal degrees of freedom were invariably excited and a 'ballooning' of the vortex core would appear (reminiscent of a vortex breakdown). Such effects are of course inaccessible to the simple model

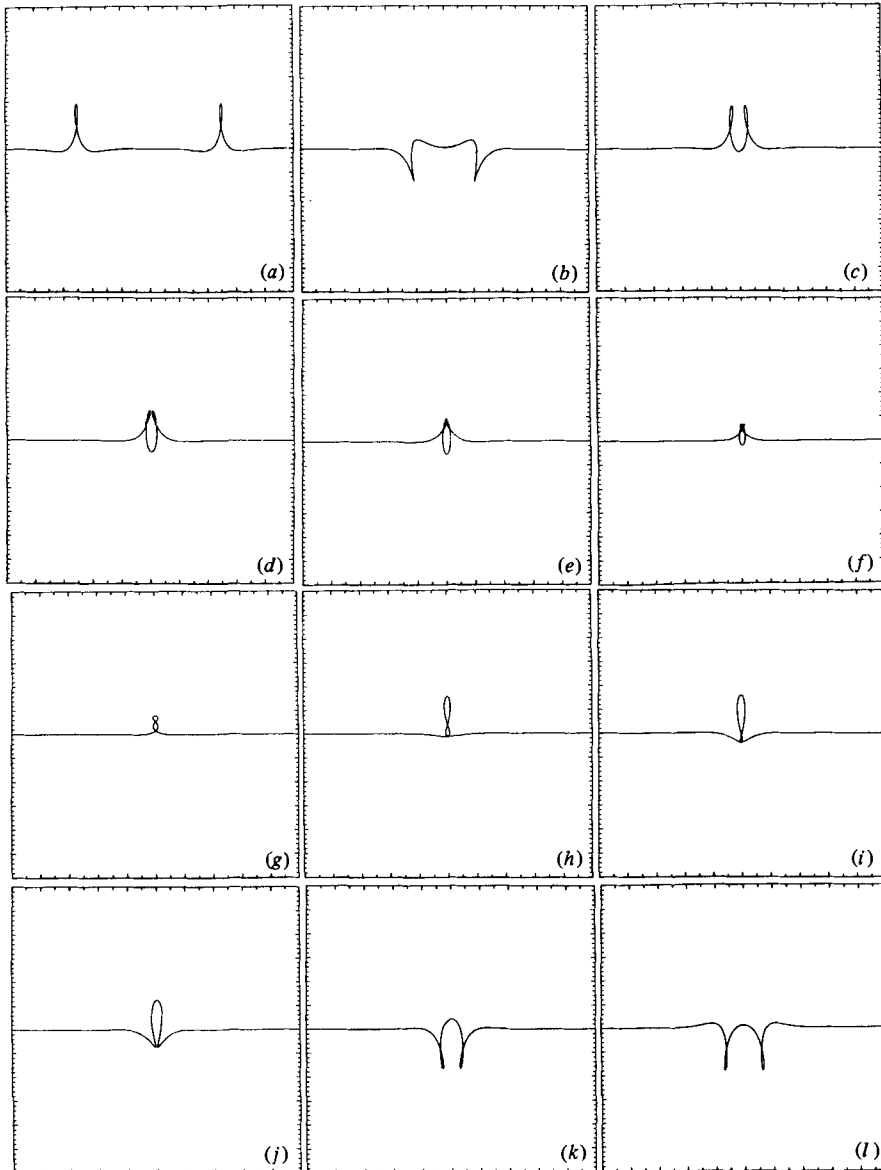


FIGURE 2. Plan view of the collision of opposite but otherwise identical solitons on a free filament evolving under LIA. Frames are not uniformly spaced in time, but were selected to show maximum detail of the collision. Time increases from (a) to (l).

under study here. In the latter study more controlled soliton (or solitary-wave) collisions could be produced. Experimental amplitudes are currently of the order of the core radius, and the dynamics of the core enters in an essential way. It is not clear at the present time how much vortex stretching goes on when the solitary waves that are observed experimentally collide. We stress that LIA and hence figures 2-6 pertain to the case of no vortex stretching. In a recent paper Levi, Sym & Wojciechowski (1983) calculate two-soliton interactions analytically and sketch a collision with two solitons very disparate in size. This is a non-trivial task, since

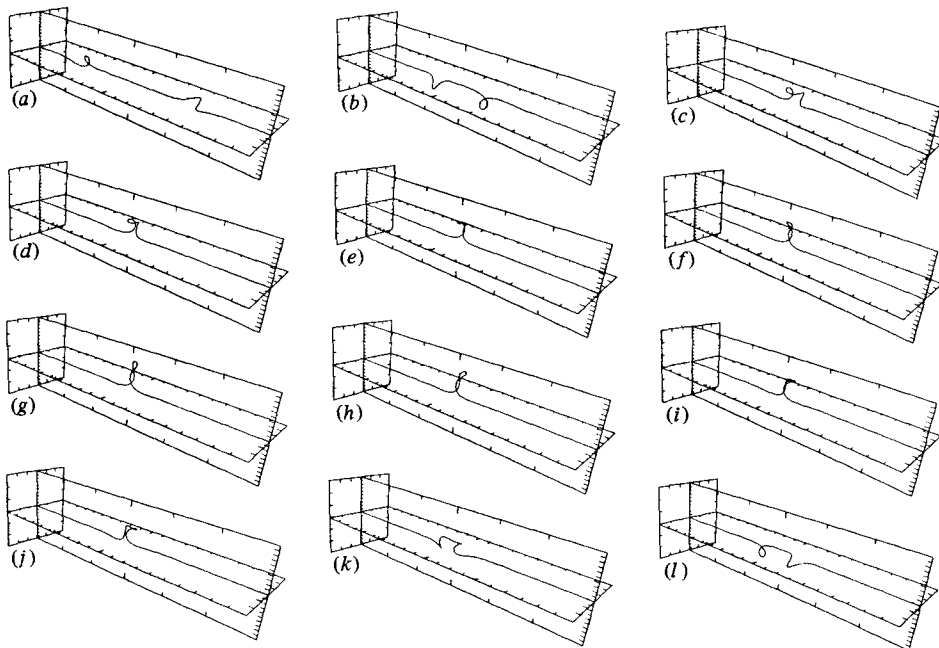


FIGURE 3. Perspective views corresponding to the plan-view frames in figure 2.

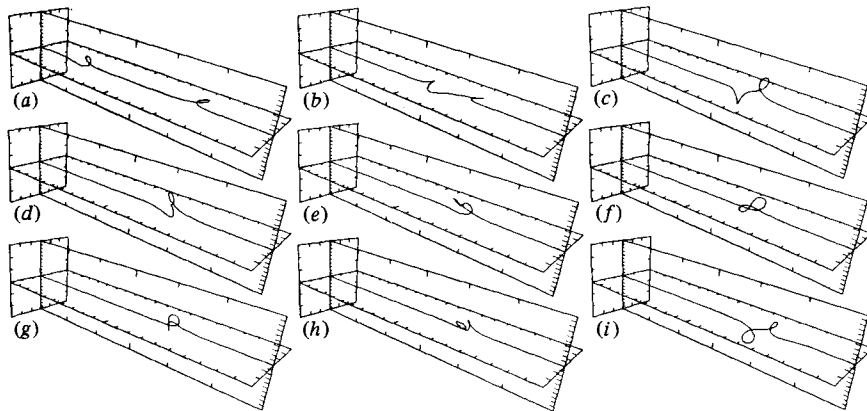


FIGURE 4. Perspective views of a head-on collision sequence between two different solitons. The high-torsion soliton starts at left, the low-torsion soliton at right. Time increases from (a) to (i).

the direct procedure of obtaining the curve shape from curvature and torsion ‘generally...requires the solution of some Riccati equation with coefficients built from $[\kappa]$ and τ' ’ (Levi *et al.* 1983).

2.4. *Dispersion of solitons in a shear flow*

Leaving the realm of analytically accessible results, we now consider a filament with solitons on it acted on by the shear of (8). The vortex is placed along the z -axis and given a perturbation in the form of one or more solitons of moderate amplitude. The objective is to describe the evolution of the filament from this initial condition.

The motivation for introducing solitons as the initial perturbation is twofold. First, from the formal theory briefly summarized in §2.1 it follows that any initial

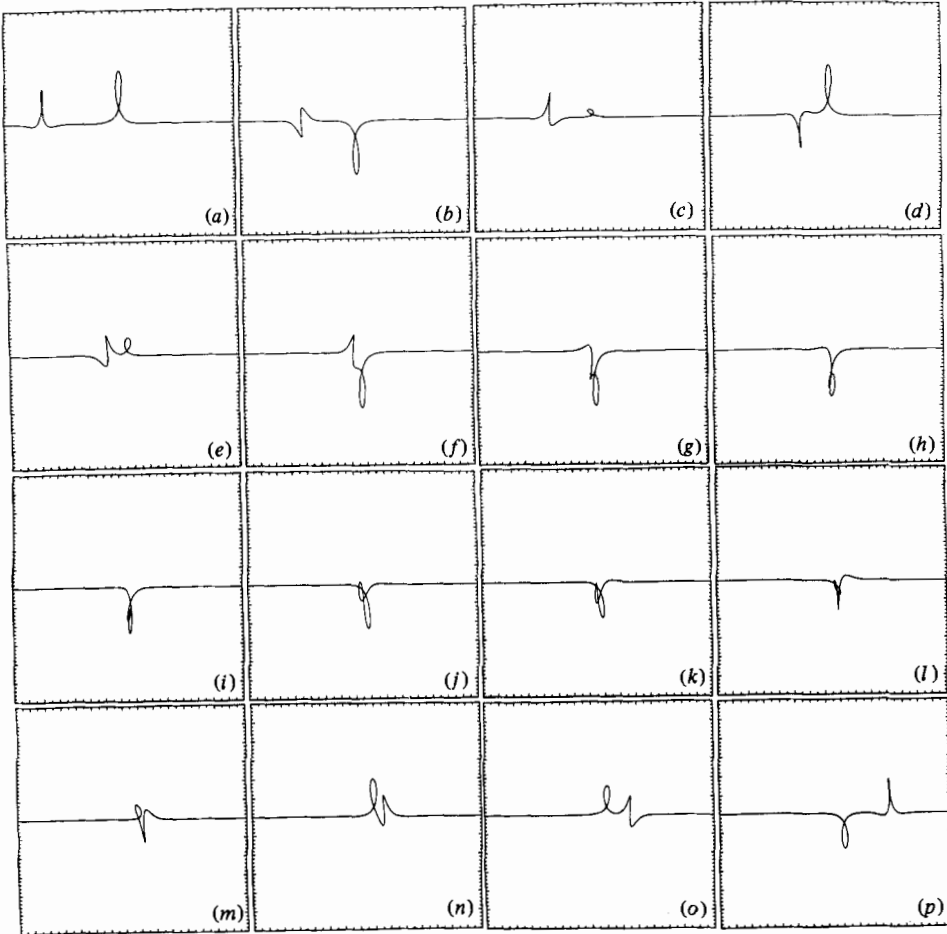


FIGURE 5. Plan views of the head-tail collision between a high-torsion soliton (starting at left) and a low-torsion soliton. Time increases from (a) to (p), and frames were again selected to show maximum detail.

perturbation of a free filament will produce one or more solitons. Thus, since solitons are the 'natural' excitations of a filament, it is reasonable to introduce them as initial data in a numerical experiment. Secondly the experiment by Hopfinger & Browand (1982) has shown that, when one has a strong vortex 'anchored' at one end in a turbulent flow, the oscillations in this turbulence are sufficient under certain circumstances to trigger soliton (or solitary-wave) disturbances on the filament. Now, in an experimental mixing-layer apparatus the two-dimensional vortex 'rollers' that evolve have both ends imbedded in turbulent boundary layers on the walls of the apparatus. It is then natural to assume that here also solitons (or solitary waves) will be triggered and will propagate across the span of the apparatus.† Thus it seemed that the mixing layer might provide a useful area of application for the ideas being pursued. Incidentally, this scenario suggests that the onset of three-dimensionality

† This scenario was first suggested to one of us (H. A) in conversations with J. Haritonidis, but had already occurred to Browand and Hopfinger (private communication), who have in fact searched for the solitons in the mixing layer, so far without observing any. It is also possible that small 'kinks' are introduced on the vortex 'rollers' by upstream disturbances in the wind tunnel.

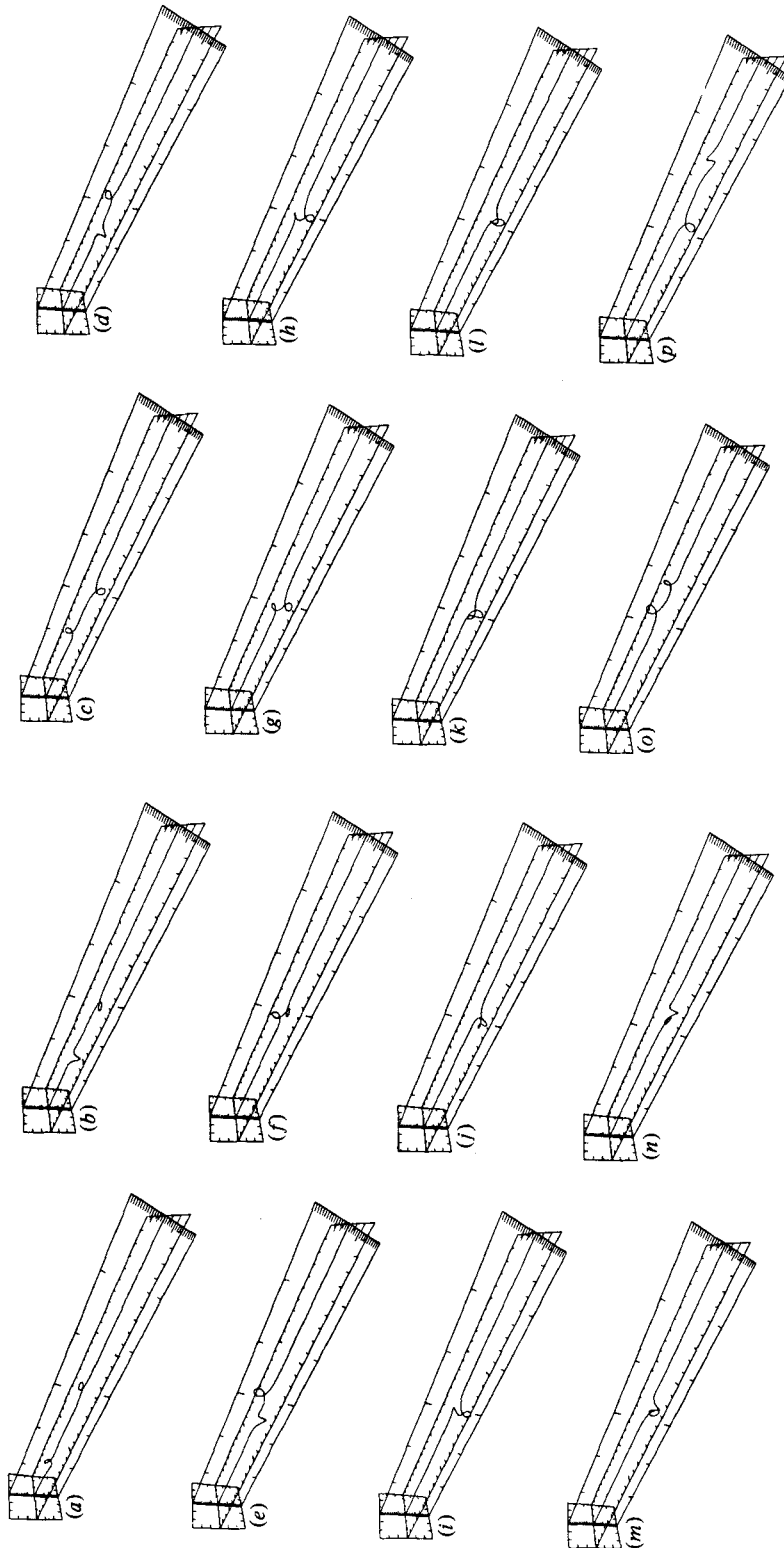


FIGURE 6. Perspective views corresponding to the frames in figure 5.

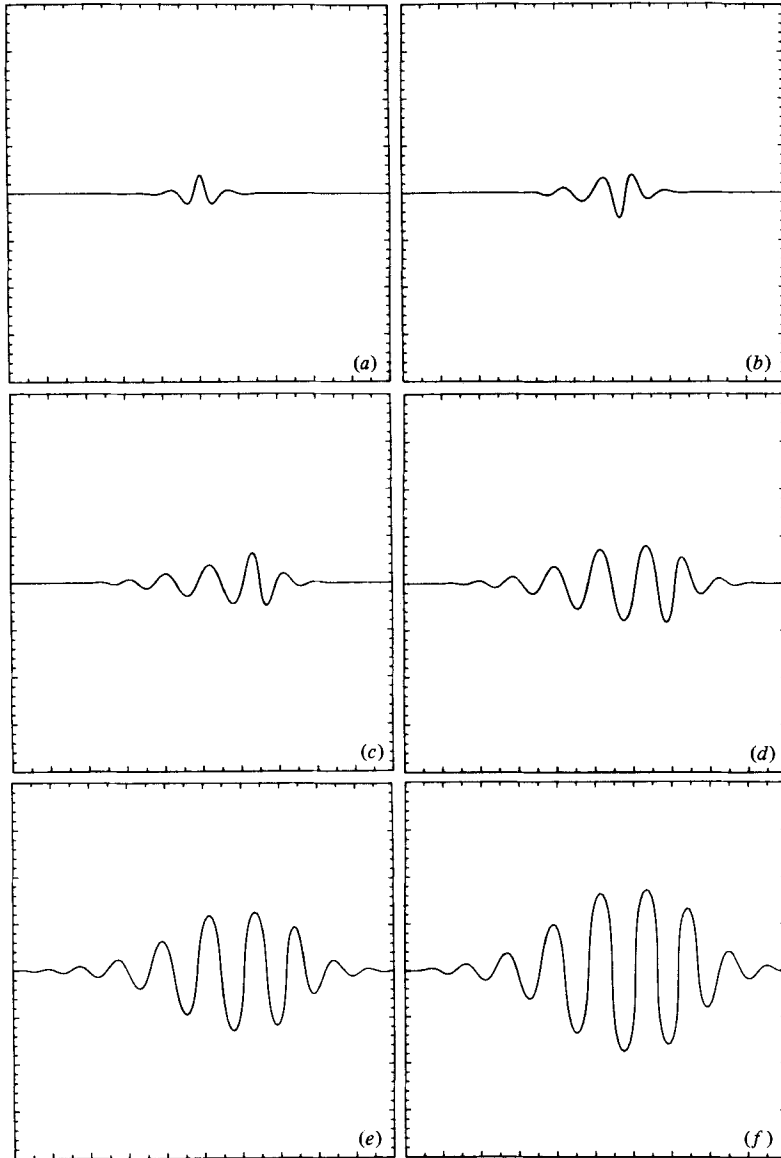


FIGURE 7. Dispersion of a high-torsion soliton by a background shear flow. Plan-view projections onto the (z, x) -plane. Along the abscissa $0 \leq z \leq 2$, along the ordinate $-0.2 \leq x \leq 0.2$ for all frames. Time increases from (a) to (f). The values of parameters U_0 and \mathcal{A} , (8), were $U_0 = 4000$, $\mathcal{A} = 5$. The torsion of the initial soliton was 36.

in mixing layers may be facility dependent and also that applying suction to the boundary layers on the sidewalls will delay the onset of three-dimensional motion.

Figure 7 shows a sequence of events in the stretching of a filament with a single high-torsion soliton on it by the shear flow (8). All views are projections on the (z, x) -plane, i.e. correspond to a spanwise view in a conventional mixing-layer apparatus. It is immediately apparent that the soliton starts emitting a train of waves on the filament, and that these waves are being continually stretched by the background advection. This point is amplified in figure 8, where the filament

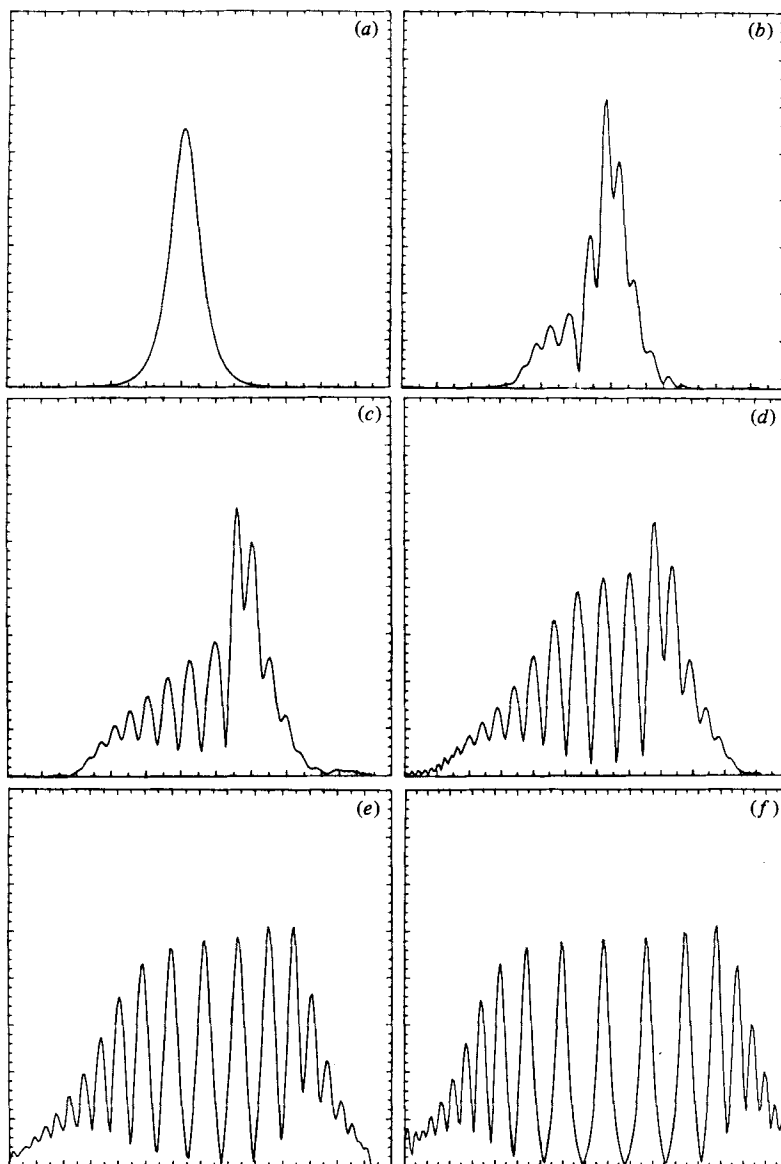


FIGURE 8. Plots of instantaneous filament curvature *vs.* arclength for the frames in figure 7. The curvature scale (ordinate) is the same in all frames. However, owing to stretching, the total arclength increases, and the scale along the abscissa is adjusted accordingly (from $0 \leq s \leq 2.2$ in (a) to $0 \leq s \leq 3.4$ in (f)).

curvature is plotted *vs.* arclength. The initial single bump (figure 8a) corresponding to the soliton is seen to become surrounded by and eventually yield to a succession of bumps corresponding to the dispersing waves. At late times the waves take on a finger-like appearance which is reminiscent of the pictures produced by Breidenthal (1978, 1979) of the 'wiggle' instability. In figure 9 an analogous disintegration of a low-torsion soliton is displayed. The intermediate stages are rather different, the final 'finger' pattern, however, is very similar (except for scale as discussed following (11)). The curvature signal (not shown) is not nearly as clear as for the high-torsion case in figures 7 and 8.

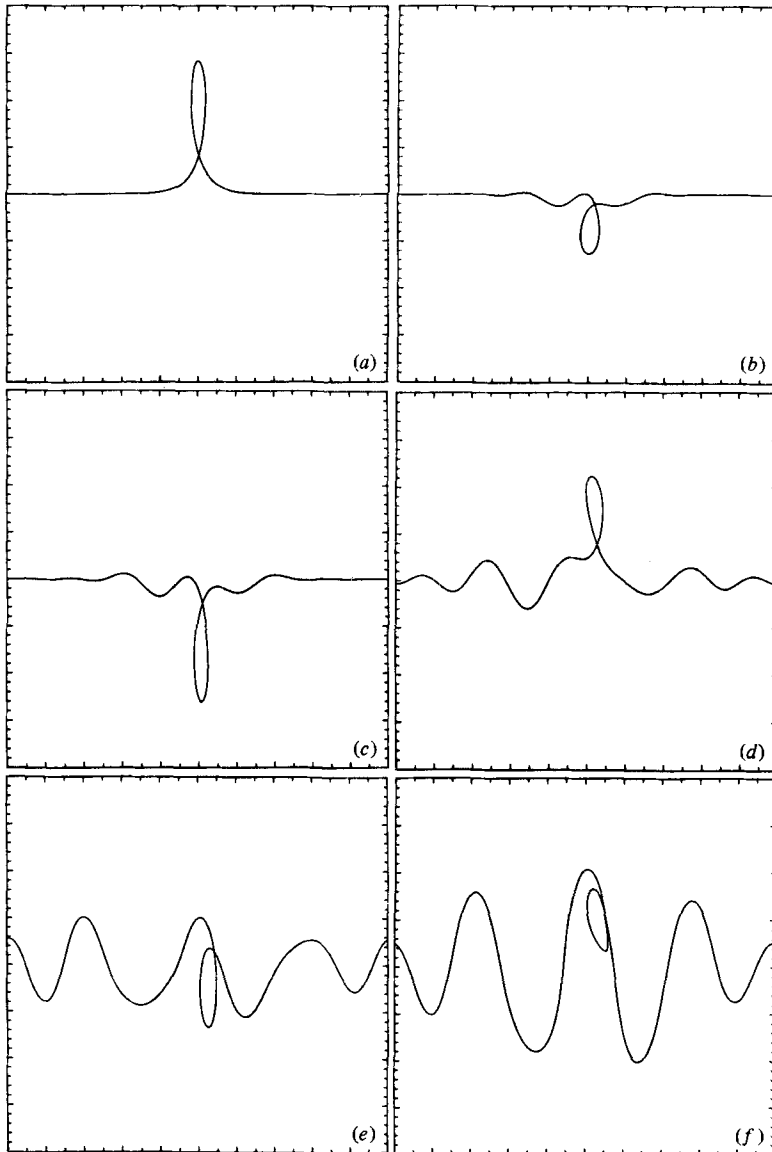


FIGURE 9. Dispersion of a low-torsion soliton by a background shear flow. This run is similar to the one in figure 7, the (z, x) -window shown is the same and so is the value of \mathcal{A} . However, here $U_0 = 1000$ and the torsion of the initial soliton was only 1.

Figures 7–9 correspond to a periodic array of identical solitons (because of the periodic boundary condition in z). In figure 10 we show a more ‘realistic’ case where the initial condition consists of three randomly chosen solitons† with different values of the torsion (and thus also different directions of propagation). Again we see the emergence of several waves, which we identify as being ‘radiated’ by the solitons (compare the results in §2.3, where the sections of filament between solitons remained unperturbed). As the waves are stretched out by the shear a rather characteristic

† It is not difficult to develop a subroutine that will initialize any (small) number of solitons of different widths and torsions selected by a random-number generator. Since the amplitude in a soliton decays to zero rapidly on both sides of the soliton there is no difficulty in placing different solitons on contiguous sections of the filament.

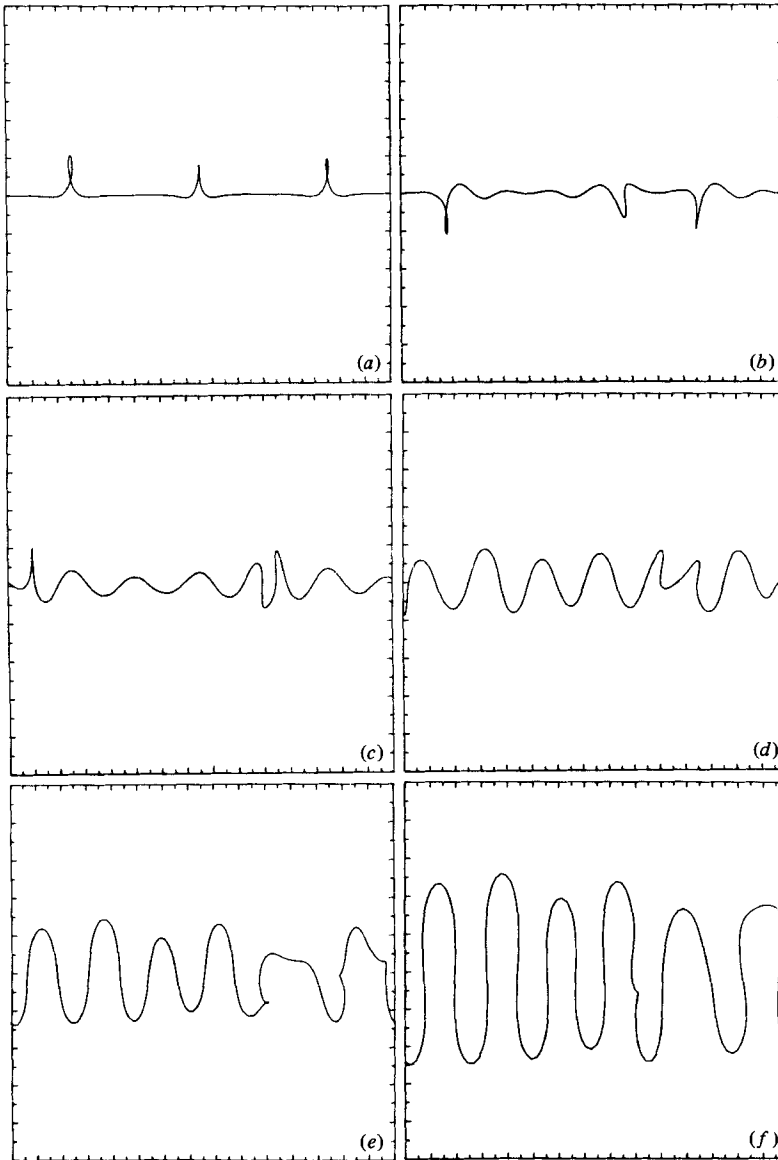


FIGURE 10. Plan views of the dispersion of three 'random' solitons by a background shear. Along the abscissa $0 \leq z \leq 3$, along the ordinate $-0.5 \leq x \leq 0.5$ in all frames. Time increases from (a) to (f). Parameters were $U_0 = 800$, $A = 5$ and (from left to right) the initial solitons had torsions $-8.2, 12.7$ and -10.1 respectively. Values of θ , (2), are (a) 0, (b) 0.010, (c) 0.021, (d) 0.036, (e) 0.048, (f) 0.065.

pattern emerges. Figure 11 gives a perspective view of this pattern corresponding to the projection shown in figure 10 (f). The resulting wavetrain has a certain well-defined periodicity with some imperfection. Apart from this modulation of spatial frequency, which is indeed also seen in Breidenthal's (1978, 1979) experimental pictures, there is clearly some amplitude modulation (which seems somewhat more pronounced than what is observed experimentally).† It should be stressed that in figures 7, 9 and 10

† A different but qualitatively similar result to figure 10 is reproduced in the review article by Laufer (1983).

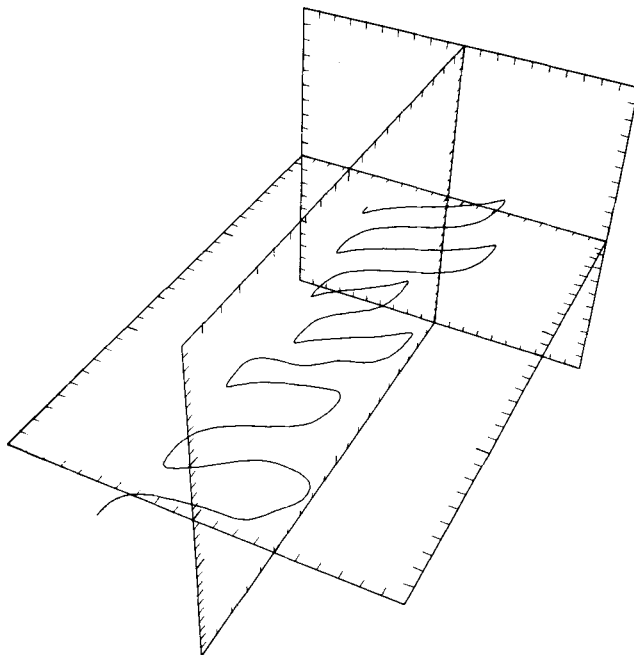


FIGURE 11. A perspective view of the filament shown in figure 10(*f*). Scales along axes of x , y and z are now the same.

remnants of the solitons may occasionally be seen during late stages of evolution (see e.g. figure 9*f*). It seems intuitively clear that vestiges of the helical twists put in initially should remain, since the imposed shear obviously contains no velocity components to ‘uncoil’ the filament, and the LIA terms in the total velocity tend to simply propagate the twist.

Our experiences with waves emanating from solitons suggest that the wavelength λ of these waves is rather insensitive to the amplitude or torsion of the solitons. If one assumes that λ depends only on the circulation Γ of the vortex and on the slope U_0/Δ of the shear-flow profile, it follows by simple dimensional reasoning that

$$\lambda \sim (\Gamma\Delta/U_0)^{\frac{1}{2}}. \quad (11)$$

We have checked this relation by varying the slope U_0/Δ of the profile by a factor of 4 ($\frac{1}{4}$) and observing, to good accuracy, a change in wavelength λ by a factor of $\frac{1}{2}$ (2). The filaments shown in figures 7, 9 and 10 were in essence always restricted to the vicinity of $x = y = 0$ and only the linear portion of the tanh in (8) was of significance. The differences in wavelength among the sequences in figures 7, 9 and 10 can all be explained in terms of (11).

For the results shown in figure 10 we have used $U_0 = 800$, $\Delta = 5$ (and $C\Gamma = 1$ as mentioned earlier). This may seem to be a very large value of U_0 , but we have observed that making U_0 smaller simply allows the solitons to pass many times through the computational domain. Finally, when the effects of the shear begin to appear, the solitons have already evolved for so long that time-stepping errors are beginning to degrade the computation. In this sense we do not look upon U_0 as a parameter that must be above some threshold for wave generation to take place. Small values of U_0 simply appear to slow down the wave-formation process. As

already mentioned, varying U_0 (from 250 to 4000) produced no qualitative changes and only altered the wavelength of the emerging waves in accordance with (11).

The wave-generation mechanism illustrated in figures 7–10 seems to us to be of intrinsic interest, since it produces an extended wavetrain with a definite (albeit modulated) spatial frequency starting from a completely localized finite-amplitude initial perturbation. We are not aware of other mechanisms that readily achieve this. Conventional attempts at theoretical explanation of the Breidenthal ‘wiggle’ typically *start* with initial perturbations in the form of extended waves and use ideas of linearized stability theory to suggest the finite-amplitude behaviour (for this approach see Pierrehumbert & Widnall 1982; Robinson & Saffman 1982, 1983; Ho & Huerre 1984).

It is clearly desirable to place this soliton wave ‘radiation’ mechanism, proposed here on the basis of numerical experiments and (11), on firmer theoretical ground. Since the waves start out by being of very small amplitude, this might be possible by calculating the infinitesimal instability of a soliton in a linear shear. The equations of motion, however, are no longer simply the LIA equations. We have developed what we believe are suitable equations, but so far we have not succeeded in carrying out the required elucidating calculation. There is clearly a close connection between our observations and recent theoretical work on other soliton-bearing equations subjected to forcing (see e.g. McLaughlin & Scott 1978). The main obstacle in making direct contact with that work is the technical issue of rewriting the shear flow (8) as a functional of the wave function in the Schrödinger equation (6). It is clear that since the background flow depends on spatial coordinates, whereas the wave function depends on intrinsic geometrical properties of the filament, any expression of the shear in terms of the wave function must involve rather complicated integral operators.

We stress that the interplay between induction and advection is essential in producing a final state such as figure 10(*f*) from the initial state figure 10(*a*). Advection alone could never lead to the delocalization along the filament that is seen in these figures. In this sense the mechanism suggested here is dynamical (as opposed to kinematical). We should also note that although similar extended wave patterns will emerge for localized initial perturbations that are not assemblies of solitons, the contrast between the results in §2.3 and those of this subsection is particularly clear for such initial conditions.

The main unsatisfactory aspect of the calculation is that the value of C is not fixed *a priori*. This means that, although we can display a sequence of geometrical shapes of the vortex filament, we have no objective way of assigning times to the frames in figure 10. We have recorded the values of the variable θ , (2), in the captions to the figure, and the reader is of course at liberty to convert them to ‘physical time’ using an assumed value for C .

3. Summary, conclusions, extensions

We have displayed results of numerical experiments on vortex-filament motion using a conceptually and computationally simple model based on LIA with and without a background advecting flow. The main virtue of this model, due originally to Hama (1963), is that it reduces to the integrable cubic Schrödinger equation for a free filament. Our main conclusions are as follows.

1. Phenomenologically soliton (or solitary-wave) excitations play a role in the evolution of thin, strong vortex filaments both in the laboratory and in Nature.
2. Such excitations can be simulated using the LIA. Some of the complex patterns

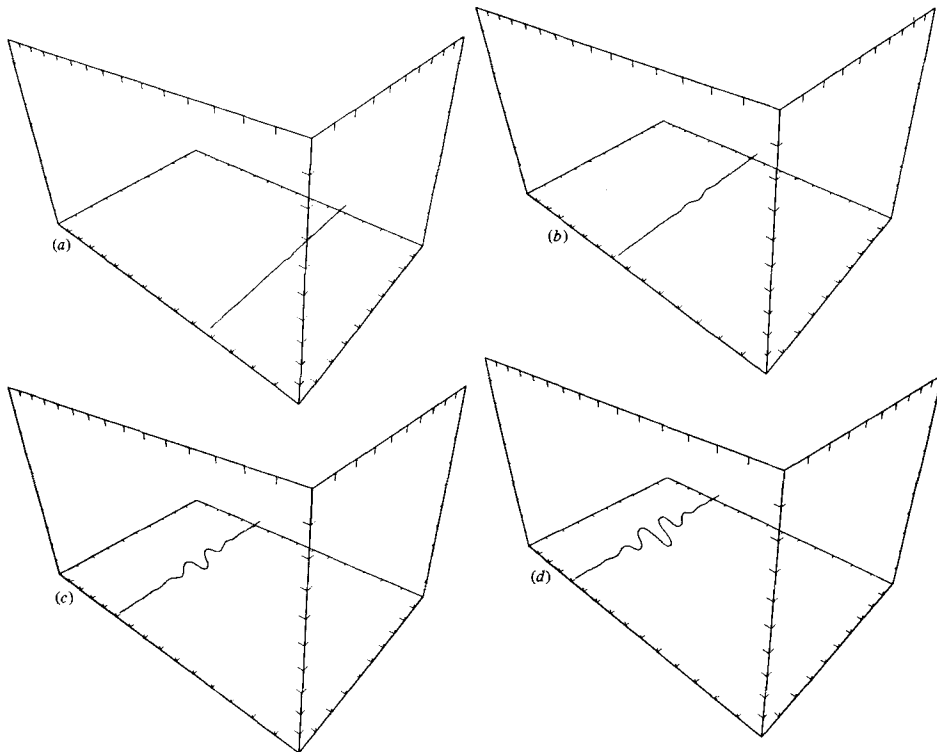


FIGURE 12. Perspective views of the evolution of a vortex filament in a boundary-layer background flow as it is swept downstream. The filament was initially given a small-amplitude, localized, one-sided deflection (frame (a)). Various secondary 'wiggles' appear, possibly resembling the vortex structure in a boundary-layer 'spot'.

of soliton interactions have been elucidated. The idealization of a vortex filament as a space curve implies, in particular, that modes of excitation that involve the degrees of freedom of the vortex core, such as axisymmetric waves, are not accommodated by the model.

3. When subjected to a background shear, LIA solitons disperse into a family of waves. This mechanism, which produces an extended wavetrain from an initially localized finite-amplitude perturbation of the vortex filament, yields filament shapes with a qualitative resemblance to the 'wiggly' vortices visualized by Breidenthal (1978, 1979) in the mixing layer. The mean wavelength expected within such a dispersive wavetrain is given by (11).

It is tempting to extend the modelling from free shear flows to boundary-layer flows, as was indeed Hama's (1963) original motivation. The simplest way to do this is to replace U_{ext} in (7) by a Blasius profile. However, the question of how to enforce the boundary condition of a rigid wall arises. So long as the filament does not approach the wall very closely, it is inconsistent to include an image vortex, since the basic assumption of LIA is that local induction dominates over any other velocities induced by remote sections of the filament. When such a model is pursued, however, one all too frequently finds that parts of the filament do indeed approach and ultimately pass through the wall after some time, and the remainder of the calculation becomes meaningless. Nevertheless, we have performed several calculations of this kind in an attempt to model wiggly vortices in boundary-layer flows (such

as the so called ‘horshoe’ or ‘hairpin’ or ‘ Λ ’ vortices). And although the model is physically unsatisfactory for several reasons, we conclude by showing one set of rather typical results because they are highly suggestive.

Figure 12 shows the results of a simulation in which an initially straight filament in a model† boundary-layer velocity field was given a small localized perturbation (figure 12*a*) as if by a protrusion in the bounding wall. The combination of transverse perturbation and its attendant LIA velocity and the background shear leads to a dispersive wavetrain by the mechanism discussed in §2.4 (except that now the background flow is not antisymmetric in y). As the filament evolves, the localized perturbation is seen to develop into a concentrated wave packet that we conjecture may resemble the vorticity structure in a boundary-layer spot. The calculation shown in figure 12 is physically consistent. However, in figure 12(*d*) the rearward portion of the filament closest to the bounding wall has in fact just touched the wall, and in the next time step will dip below $y = 0$.

We submit that simple models such as those studied here, however simplistic they may appear from the point of view of the complete equations of motion, are useful in suggesting patterns of evolution in fully nonlinear flow regimes. We believe that model calculations can be used as a valuable guide for more comprehensive numerical experiments. We hope that model results such as these will suggest analytical methods for understanding vortex flows starting from the fundamental equations. This is, of course, the ultimate goal.

We are indebted to Dr J. H. Golden for sending us pictures and ciné films of tornadoes and waterspouts. This work was supported in part by NSF grant MEA81-16910 to Brown University, by the Allied Foundation and by the Exxon Education Foundation. Use of the VAX-11/780 facility within the Division of Engineering at Brown and a grant of computer resources by the Scientific Computing Division at NCAR are gratefully acknowledged. NCAR is sponsored by NSF.

REFERENCES

- AREF, H. 1983 Integrable, chaotic, and turbulent vortex motion in two-dimensional flows. *Ann. Rev. Fluid Mech.* **15**, 345–89.
- ARMS, R. J. & HAMA, F. R. 1965 Localized-induction concept on a curved vortex and motion of an elliptic vortex ring. *Phys. Fluids* **8**, 553–559.
- BATCHELOR, G. K. 1967 *Introduction to Fluid Dynamics*, pp. 509–511. Cambridge University Press.
- BETCHOV, R. 1965 On the curvature and torsion of an isolated vortex filament. *J. Fluid Mech.* **22**, 471–479.
- BREIDENTHAL, R. 1978 A chemically reacting, turbulent shear layer. Ph.D. thesis, California Institute of Technology.
- BREIDENTHAL, R. 1979 Chemically reacting, turbulent shear layer. *AIAA J.* **17**, 310–311.
- DHANAK, M. R. & BERNARDINIS, B. DE 1981 The evolution of an elliptic vortex ring. *J. Fluid Mech.* **109**, 189–216.
- DONNELLY, R. J. 1967 *Experimental Superfluidity*. University of Chicago Press.
- EISENHART, L. P. 1960 *A Treatise on the Differential Geometry of Curves and Surfaces*, §§13–15. Dover.
- GOLDEN, J. H. & PURCELL, D. 1978 Life cycle of the Union City, Oklahoma tornado and comparison with waterspouts. *Mon. Weather Rev.* **106**, 3–11.
- HAMA, F. R. 1963 Progressive deformation of a perturbed line vortex filament. *Phys. Fluids* **6**, 526–534.

† The background was not exactly a Blasius profile, but for convenience one of the common approximations given in terms of known elementary functions.

- HARDIN, J. C. 1982 The velocity field induced by a helical vortex filament. *Phys. Fluids* **25**, 1949–1952.
- HASIMOTO, H. 1972 A soliton on a vortex filament. *J. Fluid Mech.* **51**, 477–485.
- HO, C.-M. & HUERRE, P. 1984 Perturbed free shear layers. *Ann. Rev. Fluid Mech.* **16**, 365–423.
- HOPFINGER, E. J. & BROWAND, F. K. 1982 Vortex solitary waves in a rotating, turbulent flow. *Nature* **295**, 393–395.
- HOPFINGER, E. J., BROWAND, F. K. & GAGNE, Y. 1982 Turbulence and waves in a rotating tank. *J. Fluid Mech.* **125**, 505–534.
- KIDA, S. 1981 A vortex filament moving without change of form. *J. Fluid Mech.* **112**, 397–409.
- KIDA, S. 1982 Stability of a steady vortex filament. *J. Phys. Soc. Japan* **51**, 1655–1662.
- LAMB, G. L. 1977 Solitons on moving space curves. *J. Math. Phys.* **18**, 1654–1661.
- LAUFER, J. 1983 Deterministic and stochastic aspects of turbulence. *Trans. ASME E: J. Appl. Mech.* **50**, 1077–1083.
- LEIBOVICH, S. & MA, H. Y. 1983 Soliton propagation on vortex cores and the Hasimoto soliton. *Phys. Fluids* **26**, 3173–3179.
- LEVI, D., SYM, A. & WOJCIECHOWSKI, S. 1983 N -solitons on vortex filament. *Phys. Lett. A* **94**, 408–411.
- MAXWORTHY, T., HOPFINGER, E. J. & REDEKOPP, L. G. 1985 Wave motions on vortex cores. *J. Fluid Mech.* (to be published).
- MCLAUGHLIN, D. W. & SCOTT, A. C. 1978 Perturbation analysis of fluxon dynamics. *Phys. Rev. A* **18**, 1652–1680.
- PETERSON, R. E., MINOR, J. E., GOLDEN, J. H. & SCOTT, A. C. 1979 A rare close up of an Australian tornado. *Weatherwise* **32**, 188–193.
- PIERREHUMBERT, R. T. & WIDNALL, S. E. 1982 The two- and three-dimensional instabilities of a spatially periodic shear layer. *J. Fluid Mech.* **114**, 59–82.
- ROBINSON, A. C. & SAFFMAN, P. G. 1982 Three-dimensional stability of vortex arrays. *J. Fluid Mech.* **125**, 411–427.
- ROBINSON, A. C. & SAFFMAN, P. G. 1984 Three-dimensional stability of an elliptical vortex in a straining field. *J. Fluid Mech.* **142**, 451–466.
- SHAMPINE, L. F. & GORDON, M. K. 1975 *Computer Solution of Ordinary Differential Equations*. Freeman.
- SPIEGEL, E. A. 1980 Fluid dynamical form of the linear and nonlinear Schrödinger equations. *Physica D* **1**, 236–240.
- WILSON, L., PEARSON, A. & OSTBY, F. P. 1979 Tornado! *Weatherwise* **32**, 27–33.
- ZABUSKY, N. J. 1981 Recent developments in contour dynamics for the Euler equations. *Ann. NY Acad. Sci.* **373**, 160–170.
- ZAKHAROV, V. E. & SHABAT, A. B. 1972 Exact theory of two-dimensional self-focusing and one-dimensional self-modulation of waves in nonlinear media. *Sov. Phys. JETP* **34**, 62–69.